Semiconductor Optical Amplifier Based Wavelength Conversion of Nyquist-16QAM for Flex-grid Optical Networks

Benoît Filion, Jiachuan Lin, An Nguyen, Xiaoguang Zhang, Sophie LaRochelle, and Leslie A. Rusch

Journal of Lightwave Technology, (Volume 34, Issue 11) (2016)

Doi: 10.1109/JLT.2016.2547894

http://ieeexplore.ieee.org/stamp/stamp.jsp?tp=&arnumber=7446281&isnumber=7452451

Semiconductor Optical Amplifier Based Wavelength Conversion of Nyquist-16QAM for Flex-grid Optical Networks

Benoît Filion, Jiachuan Lin, An Nguyen, Xiaoguang Zhang, Sophie LaRochelle, *Fellow, OSA, Senior Member, IEEE*, and Leslie A. Rusch, *Fellow, IEEE*

***Abstract*—We experimentally demonstrate semiconductor optical amplifier (SOA) based wavelength conversion of 3×25 Gbaud Nyquist-16QAM signal for a flex-grid network. The conversion efficiency and power penalty of each of three channels during single pumped SOA wavelength conversion are studied with respect to three different channel spacings (or frequency grids). The BER performance of all converted channels fall below the FEC threshold of 3.8e-3, even with a 50 GHz grid. The results show the trade-off between channel spacing, conversion efficiency and BER power penalty. Closely packed channels, which clearly increase spectral efficiency, are also shown to decrease conversion power penalty, potentially counter balancing increased crosstalk levels. These results can be used to optimize routing and spectrum allocation strategy when SOA wavelength converter(s) are present in the optical link.**

***Index Terms*—Wavelength conversion, four wave mixing, Nyquist, flex-grid, optical signal processing**

I. Introduction

COHERENT detection, advanced modulation formats, and multi-carrier signaling (OFDM and Nyquist-WDM) are widely studied in optical transmission systems [1][2]. As these technologies mature, they are expected to trickle down to metro and access networks [3]. In addition to providing higher data rates and greater per-channel spectrum efficiency (SE), these technologies also enable a flex-grid/elastic network configuration. The flex-grid configuration can adaptively select SE and bit rate at the transmitter end for each channel [4][5], allowing further improvement of the total SE of the network. In such elastic optical networks, the optical spectrum is divided into small slots (like 12.5GHz, or even 6.25GHz) [6], and then (re)allocated to each channel according to the request of bandwidth and wavelength. The flex-grid must deal with issues such as spectrum fragments and potential wavelength conflicts [7]. Deploying wavelength converters at optical connection nodes has been proposed as an effective solution [8][9]. Converters at intermediate nodes enable spectrum defragmentation and obviate the requirement for frequency-shifting transmitter laser sources, thus avoiding the associated detrimental effects of laser shifts. Wavelength converters circumvent wavelength conflicts, greatly increasing the flexibility of the routing and spectrum allocation strategy.

Four-wave mixing (FWM) in nonlinear devices is often proposed for wavelength conversion of signals with phase modulation because it is transparent to bit rate and modulation format. Various nonlinear media have been studied for FWM, such as highly nonlinear fiber [10], silicon waveguides [11], silicon nanowires [12], and semiconductor optical amplifiers (SOA) [13]. Among these approaches, the SOA solution provides a practical implementation with wide spectral range, low pump power, small form factor and high conversion efficiency (CE).

Wavelength converters typically exhibit wavelength dependent performance; in a flex-grid WDM system this complicates the overall trade-off of wavelength conversion with respect to reach, bit rate and SE. Foreknowledge of these trade-offs in the presence of wavelength converter will allow the routing and spectrum allocation algorithm to cope with a complex scenario of advanced modulation, multi-wavelength and flex-grid. For Nyquist-WDM, which can easily support a flex-grid network, the conversion penalty is of particular interest.

For the first time, to the best of our knowledge, we examine experimentally the performance of SOA based wavelength conversion of Nyquist-16QAM in a flex-grid optical network. In [14] this was examined via simulation for a fixed grid of ~28 GHz; we study the impact of grid spacing on performance as well. We demonstrate BER below the forward error correction (FEC) threshold of $3.8\text{x}10^{-3}$ [15] for all three converted channels in a 3×25 Gbaud superchannel. CE is found to be a poor predictor of power penalty. BER results show that more closely spaced channels minimize the power penalty for all the

This paragraph of the first footnote will contain the date on which you submitted your paper for review. This work was supported in part by the China Scholarship Council which facilitated the exchange and collaboration between Université Laval and BUPT, and by the Natural Sciences and Engineering Research Council (NSERC) of Canada.

Jiachuan Lin (on leave from the Beijing University of Post and Telecommunications, Beijing, China, linjiachuan@bupt.edu.cn), Benoit Filion (benoit.filion.2@ulaval.ca), Sophie LaRochelle (Sophie.Larochelle@gel.ulaval.ca), and Leslie Rusch (rusch@gel.ulaval.ca) are with the Electrical and Computer Engineering Department and the Centre for Optics, Photonics and Lasers at Univ. Laval. An Nguyen has left Université Laval and joined Infinera, Santa Clara, USA (e-mail: anguyen@infinera.com).

Xiaoguang Zhang (xgzhang@bupt.edu.cn) is with the Beijing University of Post and Telecommunications, Beijing, China.

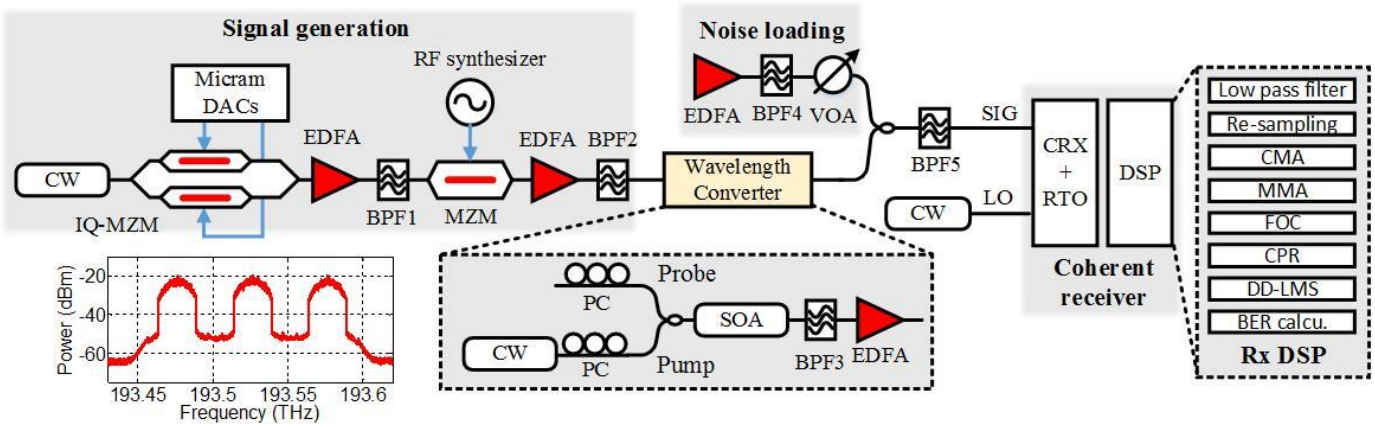

Fig. 1. : Experimental setup showing the transmitter (left) with the spectrum of three Nyquist channels with 50GHz spacing (inset), the coherent receiver (right) with the DSP flow chart, and details of the wavelength converter (top).

channels. We discuss how the performance of the three channels can be manipulated for uniformity and for overall spectral efficiency.

II. Experimental Setup

Figure 1 shows the experimental setup, which is composed of four parts: signal generation, wavelength conversion, noise loading for BER measurement, and coherent detection.

The transmitted signal carrying 16QAM data is pre-programmed and digitally pulse shaped using offline DSP. The digital pulse shaping filter is implemented by a 128-order raised cosine function with 2 samples per symbol (SPS). The roll-off factor is set to 0.01 to create a Nyquist pulse with 25.25 GHz bandwidth. The in-phase and quadrature samples are then down sampled to 1.3 SPS and loaded to two synchronized 6 bits digital-to-analog converters (Micram-DACs VEGA II) working at 32.5 GSa/s to generate 25 Gbaud electrical signals. These electrical signals are then applied to an I-Q Mach-Zehnder modulator (IQ-MZM) to modulate continuous wave (CW) light from a tunable laser source (TeraXion PS-TNL) at 193,526.8 GHz (1549.1 nm). The modulated optical signal is amplified by an erbium doped fiber amplifier (EDFA) and filtered by a 40 GHz optical band-pass filter (BPF1 – Finisar Waveshaper 4000S) to reject the spectral replicas caused by digital up-sampling.

The data modulated Nyquist signal is sent to an intensity-MZM driven by an electrical clock source (RF synthesizer) to generate three identical channels with RF spacing controlled by the clock frequency. The bias of the MZM and the amplitude of the clock source are adjusted to equalize the power levels of the three channels. BPF2 (Alnair Labs BFV-200-SM-FA) is employed for rejecting higher order channels on both sides. An inset to Fig. 1 shows the three Nyquist pulses, in this case with channel spacing of 50 GHz. The optical signal-to-noise ratio (OSNR) is above 40 dB, but the measured electrical SNR is ~27 dB due to the in-band noise pedestal observed in the inset.

At the wavelength converter, the signal carrying three Nyquist channels, is combined with a CW laser (Cobrite DX1), called the pump, and co-propagated in the SOA (CIP SOA-XN-OEC-1550). Polarization controllers (PCs) are used to optimize the interaction between pump and signals in the SOA. The center channel (channel 2) carrier and pump wavelengths are held constant, while channel 1 and channel 3 wavelengths vary with grid spacing. The pump wavelength is fixed at 193,601.9 GHz (1548.5 nm), ~75 GHz (0.6 nm) away from the center channel, 193,526.8 GHz (1549.1 nm), of the input signals.

In [13] we showed that even in the presence of a strong pump, the patterning effect is still present at the SOA output. Due to this effect, a careful optimization of the signal and pump power is required to trade-off conversion efficiency and induced non-linearities. The total signal power at the SOA input, i.e., 3 channels, is set to -12 dBm while the pump power is 8 dBm. Two isolators (not shown in Fig. 1) are used at the input and output of the SOA to avoid back reflections. The conjugate idle signals generated by FWM are located on the lower wavelength side of the pump. After the SOA, an optical filter (BPF3 - Alnair Labs BFV-200-SM-FA) is used to suppress the pump and probe, and deliver the wavelength converted signal. The converted signal is then amplified by an EDFA.

The wavelength converted signal is combined with ASE noise coming from a noise loading stage - an EDFA followed by a 1 nm optical filter (BPF4) and a variable optical attenuator (VOA). To enhance the performance of our integrated coherent receiver (CRx), the converted signal power is kept fixed at -3 dBm. To reduce noise and enhance OSNR for this input power level, we use a programmable optical filter (Finisar Waveshaper 1000S) with 50 GHz bandwidth centered on the Nyquist signal to be examined. Channel selection is done in the electrical domain. The local oscillator (LO), a tunable laser source (TeraXion PS-TNL), has 13 dBm mean power. All laser sources used in the setup have linewidth below 100 kHz. The resulting electrical signal is sampled by a real time oscilloscope (RTO) at 80 GSa/s with 30 GHz electrical bandwidth.

The sampled electrical signal is processed offline by digital signal processing (DSP) using MATLAB™. The DSP flowchart is shown in Fig.1. The signal is first filtered with a 10th order super-Gaussian low pass filter of 25.4 GHz bandwidth to reject out of band noise and adjacent channels. Due to the strong filtering of the limited DAC bandwidth and cascaded narrow optical filters, timing recovery is challenging in this scenario; we therefore use a two stage adaptive equalization scheme for joint convergence and timing [16]. We first apply a $T/4$-spaced (T: symbol period) constant modulus algorithm

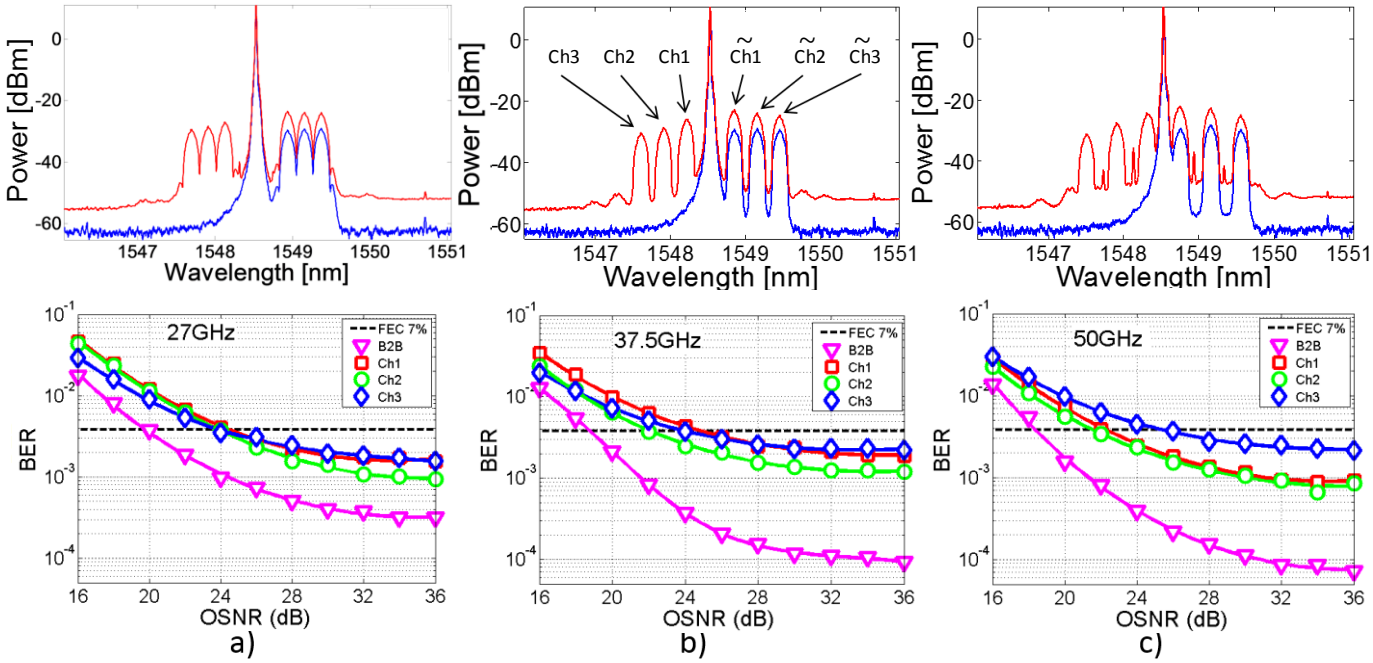

Fig. 2 Channel frequency spacing is a) 27 GHz b) 37.5 and c) 50 GHz. First row is optical spectra at the SOA input (blue, single sided) and output (red, double sided); the tilde notation refers to channels before wavelength-conversion. Second row is BER vs. OSNR; markers are measured data, while smooth curves are a rational polynomial fit of measurements.

(CMA) adaptive filter with 64 complex-valued taps for pre-convergence and timing recovery. Afterward, the signal is down sampled to 2 SPS, and then another *T*/2-spaced multi-modulus algorithm (MMA) adaptive filter is used for fine convergence to further improve SNR [17]. The frequency offset is compensated in two steps: FFT-based coarse estimation followed by a minimum mean square error algorithm for fine tuning [18]. The carrier phase is recovered by blind phase search (BPS) with 64 test angles and a block length of 65 [19]. To further reduce the residual inter symbol interference (ISI) and noise, a pair of *T*-spaced decision directed least mean squares (DD-LMS) filters are applied on the in-phase and quadrature components separately. Finally, the equalized constellation is demodulated to binary streams for BER calculation. A pseudorandom bit sequence (PRBS) of length 2^{15}-1 was used, and over 5×10^6 bits were captured.

III. Results

Flex-grid networks strive to optimize spectral efficiency and throughput by tweaking many parameters, including spacing of constituent Nyquist pulses. We investigate the performance of wavelength conversion as a function of channel spacing in terms of BER, CE and OSNR penalty. The optical spectra of the SOA input and output and the three converted channels are shown in the upper section of Fig. 2 for frequency spacing of 27 GHz, 37.5 GHz, and 50 GHz. Each spacing defines a separate frequency grid. We denote channel 1 as that closest to the pump, channel 2 in the center, and channel 3 as that farthest from the pump. The interchannel spurious tones observable in Fig. 2c originate from the RF synthesizer as the electrical clock is not purely sinusoidal; other harmonics are also generated.

The lower section of Fig. 2 gives the measured BER vs. OSNR and reveals variation in system performance when adopting different grids. The back-to-back (B2B) curve is BER before wavelength conversion, and identical for all channels. For the 50 GHz and 37.5 GHz grid, the required OSNR to reach the FEC threshold ($3.8\text{x}10^{-3}$) is about 19 dB. Here the Nyquist pulse shaping enables negligible interchannel crosstalk (ICI), as the channel grid is much wider than the baud rate. Grid spacing of 27 GHz yields spectral efficiency 1.8 times greater than that of the 50 GHz grid, but the higher ICI will cause ~1 dB OSNR penalty at the FEC threshold. The BER floor of 1e-4 at high OSNR is due to the finite SNR of the generated signals (see noise pedestal in Fig. 1 inset).

The CE is the ratio of the conjugate power to the input signal power, with power measured via an optical spectrum analyzer with resolution bandwidth of 0.01 nm. Figure 3 shows the CE for wavelength converted channels for all three grids. Note that the measured CE is not only dependent on the signal and pump powers, but also on frequency (or wavelength) detuning between the signal and the pump [11]: the wider the detuning, the lower the CE. Because of this, the highest CE (5 dB) and lowest CE (-1.5 dB) are obtained for channel 1 (closest to pump) and channel 3 (farthest from pump), respectively, when the RF spacing is 50 GHz (see Fig. 2c). Since total channel separation is largest for the 50 GHz RF spacing case, the CE variation is also the greatest, i.e., 6.5 dB. The minimum CE variation of 2.5 dB is obtained for 27 GHz RF spacing.

The required OSNR at the FEC-threshold is found by using a rational polynomial fitting routine on the measured data. The OSNR penalty, the difference in required OSNR, is calculated and shown in Fig. 4. The largest OSNR penalty variation (4 dB spread) is found for the case of 50 GHz spacing: the lowest

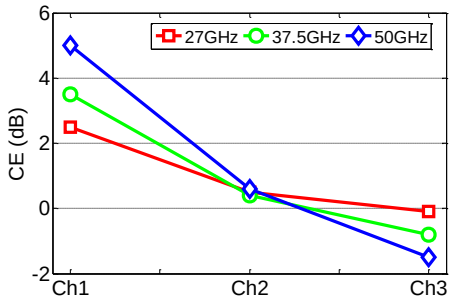

Fig. 3 Conversion efficiency per channel of the three Nyquist channels, for different frequency grids.

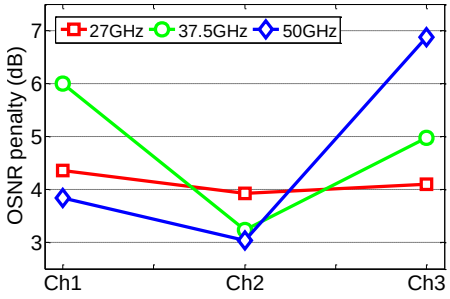

Fig. 4 OSNR penalty per channel of the three Nyquist channels, for different frequency grids.

OSNR penalty is channel 1 and the highest OSNR penalty is channel 2. For all the frequency spacings, BER performance does not follows CE performance (see Fig. 3), with channel 2 always having the lowest OSNR penalty.

IV. Discussion

A. *Power penalty vs. conversion efficiency*

While the CE for the three grids is virtually identical for channel 2, the OSNR penalty of channel 2 does vary. Similarly, the 27 GHz grid has flat power penalty across different channels, while the CE varies for this grid. Clearly the CE is not a good predictor of power penalty. This is most evident for the 50 GHz spacing where even with a 5 dB CE advantage over channel 2, channel 1 achieves higher BER than channel 2. This is due to nonlinear crosstalk and the nonuniformity of the CE over the converted signal bandwidth, as we will explain.

1) *XGM impact*

On exiting the SOA, the pump spectrum is widened due to cross-gain modulation (XGM). As highlighted in [20], this widening is much greater for phase modulated signals than intensity modulated signals. While greater conversion efficiency is achieved with close proximity of pump and signal, the pump broadening complicates this as a strategy for increasing wavelength conversion performance. As predicted in simulation of Nyquist superchannels in [14], the pulse broadening creates interference for those channels closest to the pump. While the channel closest to the pump will experience the best CE, it will also experience the worse nonlinear crosstalk from the pump XGM. The pump power in simulations in [14] was 23 dB above the signal, similar to our experimental value of 20 dB.

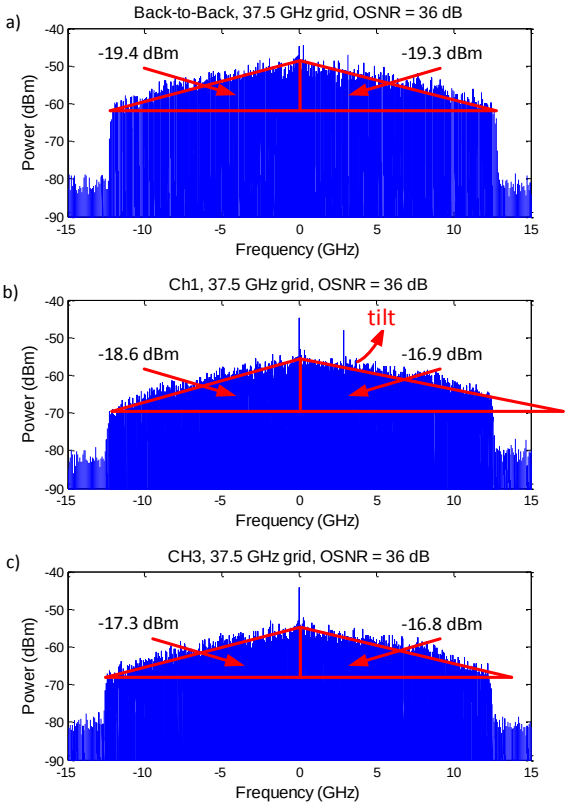

Fig. 5 Power spectrum of 37.5 GHz grid for a) B2B b) channel 1 and c) channel 3; the power on each side of the spectra (within drawn triangles) is indicated. The pump (filtered out optically) was located to the right.

2) *CE nonuniformity*

As expected, the CE in Fig. 3 decreases as the frequency detuning between the signal and the pump increases, i.e., channel 1 is best and channel 3 is worst. For high-speed signals, the intrachannel non-uniformity in the CE will induce distortions on the conjugate and impact the wavelength conversion performance. In addition, the extent of the resulting asymmetry on the conjugate power spectrum will vary with the center frequency detuning. This is explained by the different time dynamics of the optical processes, i.e., the carrier density variations, the spectral hole-burning and the carrier heating, that lead to wavelength conversion based on FWM in SOAs. Each of the optical processes impacts the FWM efficiency differently depending on the frequency detuning. For instance, at lower frequency detunings (typically below 10 GHz), the slower process (carrier density variations) will dominate the FWM efficiency. As the frequency detuning increases beyond 10 GHz, the carrier density variations contribution will become negligible and instead, the faster processes, (SHB and CH) will contribute to the wavelength conversion process up to the THz range [21].

The effects discussed can be observed in Fig. 3 where the CE drops more rapidly from channel 1 to channel 2 than from channel 2 to channel 3. For instance, with a frequency grid of 37.5 GHz, the CE is 3.2 dB lower for channel 2 compared to channel 1, but only 1.1 dB higher compared to channel 3. The same behavior can be observed by comparing each channel individually for all the frequency grids. This indicates that the asymmetry in the conjugate power spectrum, discussed in the

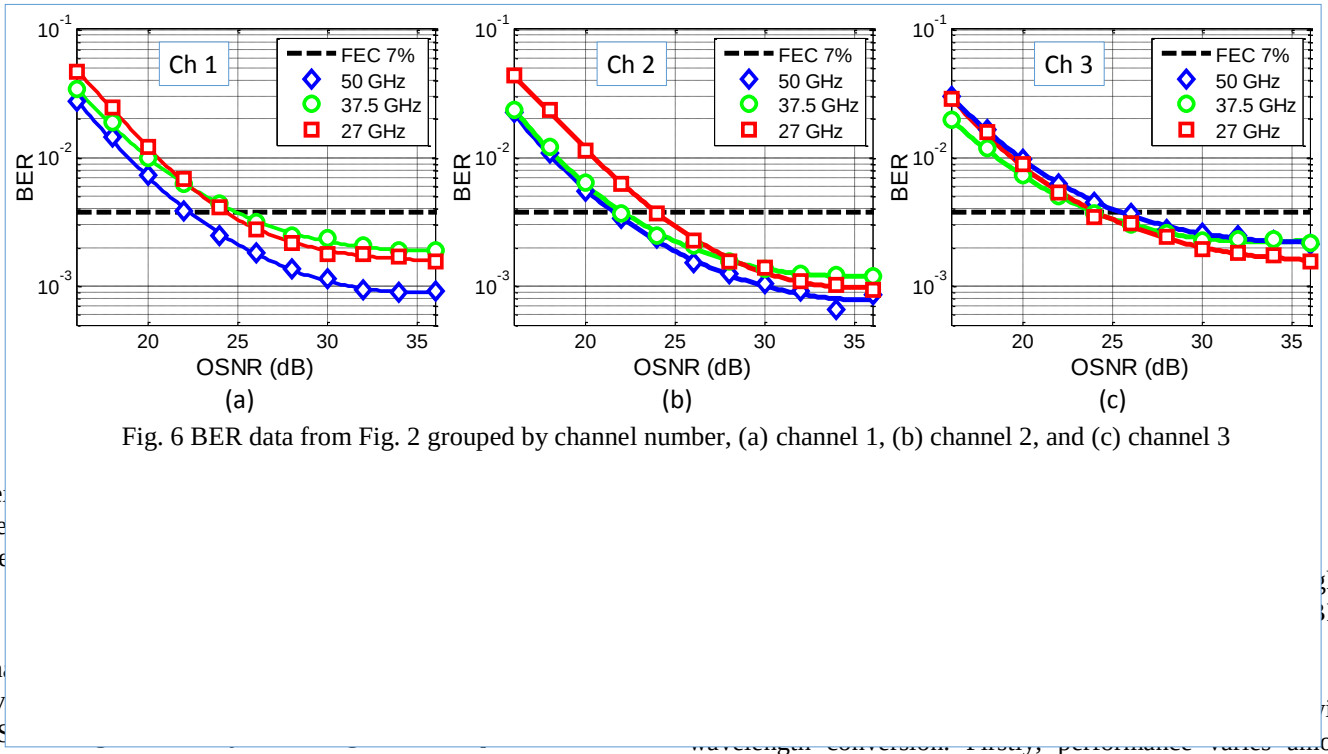

Fig. 6 BER data from Fig. 2 grouped by channel number, (a) channel 1, (b) channel 2, and (c) channel 3

slope on the right side of the channel 1 spectrum is noticeably smaller than the slope of the left side. The tilt is induced by the non-uniform intrachannel CE and the XGM. The spectrum of channel 3 is more symmetric, indicating that the slope in the CE against the frequency detuning is less significant for that channel. The asymmetry can also be quantified by the power on each side of the spectra for all the cases (see Fig. 5): the power on the right side of channel 1 is 1.7 dB higher than on the left side while it is only 0.5 dB higher for channel 3.

In Fig. 6 we present Fig. 2 BER data grouped by channel. For channel 1, closest to the pump, we see the post-conversion performance is best for large grid spacing. As the wavelength of channel 2 is fixed, larger grid spacing pushes channel 1 closer to the pump, enhancing CE. Proximity to pump also brings greater XGM nonlinear crosstalk and non-uniform CE, yet on balance channel 1 fares better at 50 GHz spacing. Inversely for channel 3, Fig. 6c, a tighter grid yields better BER for OSNRs meeting the FEC threshold. In the 27 GHz grid, channel 3 enjoys closer pump proximity and hence better performance. Note that despite the wide spread in OSNR penalty for channel 3 (see Fig. 4), the BER floors in Fig. 6c are very similar. The presence of distortion is more harmful in low OSNR regimes, leading to worse degradation at the FEC level crossing.

Focusing again on channel 1, CE goes from best to worst as we go from 50 to 27 GHz spacing; XGM is, however, worst for 50 GHz and least for 27 GHz spacing. In Fig. 6a, we see that the net effect on BER floor is 50 GHz being the most impaired channel spacing, while 27 and 37.5 GHz spacing have very similar performance. For 27 and 37.5 GHz spacing, the cumulative effects of linear inter-channel crosstalk, CE and XGM nonlinear crosstalk are comparable. Since the B2B performance is worse for 27 GHz, the OSNR penalty is actually less for this spacing sthan for 37.5 GHz, despite the similar post-conversion BER channels, and secondly, the worst case error floors are similar post wavelength conversion.

Take the case of 50 GHz spacing with a 4.5 dB spread (2.5 to 7 dB) in power penalty across channels. In order to equalize performance across channels, higher order modulations (16QAM or 64QAM) could be used for the better channel (Ch1), and more robust modulations (BPSK, QPSK) for worst channel (Ch3) when using wavelength conversion. Without varying modulation format, the overall BER of the three channel system is dominated by the weakest channel. Modulation choice would of course be subject to other criteria, such as distance to be traveled and quality of service requirements. The constraints imposed by the unequal channel performance would lead to less flexibility overall for resource allocation. A flat OSNR penalty allows both greatest flexibility and highest overall performance.

Equal power penalty (4 dB) can be achieved for all three wavelength converted channels when 27 GHz RF spacing is used. In this case, the output channel OSNR difference is small due to minimal CE variation (2.5 dB spread).Without the guard band of several GHz for the Nyquist-WDM system, the 27 GHz grid has BER dominated by crosstalk from adjacent channels; this is not the case for 50 GHz spacing. However, close spacing may be the best wavelength allocation strategy for multi-channel wavelength conversion. Without wavelength conversion, Nyquist system spacing is chosen to balance crosstalk impairment against spectral efficiency goals. However, with wavelength conversion, spectral efficiency may be even higher than expected given the positive effect of more uniform OSNR penalty at close spacing.

V. Conclusion

We experimentally study the wavelength conversion of 3×25

Gbaud 16QAM Nyquist channels with flex-grid using FWM in a SOA. BER below FEC threshold was achieved for all channels converted, even when using the widest channel spacing of 50 GHz. The study shows a performance imbalance between channels when varying the RF spacing. The wavelength conversion power penalty is least imbalanced (virtually flat) with minimal RF spacing. The study contributes to optimization of the flex-grid by taking into account wavelength conversion in the optical link.

REFERENCES

[1] K. Roberts, D. Beckett, D. Boertjes, J. Berthold, and C. Laperle, "100G and beyond with digital coherent signal processing," *IEEE Commun. Mag.*, vol. 48, no. 7, pp. 62-69, Jul. 2010.

[2] G. Bosco, V. Curri, A. Carena, P. Poggiolini and F. Forghieri, "On the Performance of Nyquist-WDM Terabit Superchannels Based on PM-BPSK, PM-QPSK, PM-8QAM or PM-16QAM Subcarriers," *J. Lightwave Technol.*, vol. 29, no. 1, pp. 53-61, Jan. 2011.

[3] H. Rohde, E. Gottwald, A. Teixeira, J. D. Reis, A. Shahpari, K. Pulverer, and J. S. Wey, "Coherent Ultra Dense WDM Technology for Next Generation Optical Metro and Access Networks," *J. Lightwave Technol.*, vol. 32, no. 10, pp. 2041-2052, May. 2014.

[4] J. K. Fischer, S. Alreesh, R. Elschner, F. Frey, M. Nolle, C. S. Langhorst, and C. Schubert, "Bandwidth-Variable Transceivers based on Four-Dimensional Modulation Formats," *J. Lightwave Technol.*, vol. 32, no. 16, pp. 2886-2895, Aug. 2014.

[5] X. Yu, M. Tornatore, M. Xia, J. Wang, J. Zhang, Y. Zhao, J. Zhang, and B. Mukherjee, "Migration from Fixed Grid to Flexible Grid in Optical Networks", *IEEE Commun. Mag.*, vol. 53, no. 2, pp. 34-43, Feb. 2015.

[6] "Draft revised G.694.1 version 1.3," Unpublished ITU-T Study Group 15, Question 6.

[7] M. Jinno, B. Kozicki, H. Takara, A. Watanabe, Y. Sone, T. Tanaka, and A. Hirano, "Distance-Adaptive Spectrum Resource Allocation in Spectrum-Sliced Elastic Optical Path Network," *IEEE Commun. Mag.*, vol. 48, no. 8, pp. 138-145, Aug. 2010.

[8] D. J. Geisler, Y. Yin, K. Wen, N. K. Fontaine, R. P. Scott, S. Chang, and S. J. B. Yoo, "Demonstration of Spectral Defragmentation in Flexible Bandwidth Optical Networking by FWM," *IEEE Photon. Technol. Lett.*, vol 23, no.24, pp. 1893-1895, Dec. 2011.

[9] N. Sambo, F. Paolucci, G. Meloni, F. Fresi, L. Potì, and P. Castoldi, "Control of Frequency Conversion and Defragmentation for Super-Channels," *J. OPT. COMMUN. NETW.*,vol 7, no.1, pp. A126-A134, Jan. 2015.

[10] E. Temprana, V. Ataie, A. Peric, N. Alic, and S. Radic, "Wavelength Conversion of QPSK Signals in Single-Pump FOPA with 20 dB Conversion Efficiency," *in Proc. OFC*, San Francisco, California, 2014, Th1H.2.

[11] C. Gui, L. Chao, Y. Qi, W. Jian, "Experimental Demonstration of Silicon Vertical Slot Waveguides for Ultra-wide Bandwidth 1.8-Tbit/s (161 WDM 11.2-Gbit/s OFDM 16-QAM) Data Transmission," *in Proc. OECC/ACOFT*, Melbourne, 2014, pp. 514.

[12] D. Vukovic, J. Schroeder, Y. Ding, M. D. Pelusi, L. B. Du, H. Ou, and C. Peucheret, "Wavelength Conversion of DP-QPSK Signal in a Silicon Polarization Diversity Circuit," *IEEE Photon. Technol. Lett., vol 27, no.4, pp. 411-414, Feb. 2015*.

[13] B. Filion, W. C. Ng, A. T. Nguyen, L. A. Rusch and S. LaRochelle, "Wideband wavelength conversion of 16 Gbaud 16-QAM and 5 Gbaud 64-QAM signals in a semiconductor optical amplifier," *Opt. Express*, vol. 21, no. 17, pp. 19825-19833. Aug. 2013.

[14] S. T. Naimi, S. P. O Duill, and L. P. Barry, "All Optical Wavelength Conversion of Nyquist-WDM Superchannels Using FWM in SOAs," J. Light. Technol., vol. 33, no. 19, pp. 3959–3967, Oct. 2015.

[15] A. H. Gnauck, P. J. Winzer, S. Chandrasekhar, X. Liu, B. Zhu, and D. W. Peckham, "Spectrally Efficient Long-Haul WDM Transmission Using 224-Gb/s Polarization-Multiplexed 16-QAM," J. Light. Technol., vol. 29, no. 4, pp. 373–377, Feb. 2011.

[16] K. Kikuchi, "Clock recovering characteristics of adaptive finite-impulse-response filters in digital coherent optical receivers," *Opt. Express*, vol. 19, no. 6, pp. 5611-5619. Jan. 2011.

[17] I. Fatadin, D. Ives, and S. J. Savory, "Blind Equalization and Carrier Phase Recovery in a 16-QAM Optical Coherent System" *J. Lightwave Technol.*, vol. 27, no. 15, pp. 3042-3049, Aug. 2009.

[18] M. Selmi, Y. Jaouen, P. Ciblat, "Accurate Digital Frequency Offset Estimator for Coherent PolMux QAM Transmission Systems," *in Proc. ECOC*, Vienna, 2009, P.3.08.

[19] T. Pfau, S. Hoffmann, and R. Noé, "Hardware-Efficient Coherent Digital Receiver Concept With Feedforward Carrier Recovery for-QAM Constellations," *J. Lightwave Technol.*, vol. 27, no. 8, pp. 989-998, Apr. 2009.

[20] Y. BenM'Sallem, C. Park, S. LaRochelle, and L. Rusch, "Multi-Format Wavelength Conversion Using Quantum Dash Mode-Locked Laser Pumps," *MDPI Photonics*, vol. 2, p. 527-539.

[21] Mecozzi, S. Scotti, A. D'Ottavi, E. Iannone, and P. Spano, "Four-wave mixing in traveling-wave semiconductor amplifiers," IEEE J. Quantum Electron., vol. 31, no. 4, pp. 689-699, Apr. 1995.

Benoît Filion was born in 1983. He received the B.S. degree in 2009, M.S. degree in 2011 and Ph.D degree in electrical engineering from Université Laval in Canada. He is currently a research associate and lab manager at the Centre d'Optique, Photonique et Laser (COPL), Université Laval, Québec, Canada.

Jiachuan Lin received his B.S. and M.S. degrees from Ocean University of China and Beijing University of Posts and Telecommunications in 2010 and 2012 respectively. Currently, he is a PhD student in electronic science and technology at the Institute of Information Photonics and Optical Communications, Beijing University of Posts and Telecommunication. He was also the exchanging Ph.D. student of Université Laval, Quebéc, QC, Canada from 2014 to 2015. His current research interest is related to the field of optical communications, also including optical frequency comb generation, and superchannel transmission systems.

An T. Nguyen was born in 1982. He received the B.S. degree in physics in 2003 and M.S. degree in electronics engineering in 2007 from University of Science – Vietnam National University (VNU) in Ho Chi Minh City, Vietnam.

From 2008 to 2011, he was pursuing his Ph.D. degree in optical telecommunications at the Centro di Eccellenza per l'Ingegneria dell'Informazione, della Comunicazione e della Percezione (CEIICP) of Scuola Superioré Sant'Anna, Pisa, Italy. His research topics involved ultra-fast (640Gbps and beyond) OTDM subsystems, multifunctional hybrid add/drop node for OTDM and WDM integration, all-optical wavelength and modulation format converter, ultrafast packet switching and photonic digital processing circuits. From 2012 to 2015, he was a post-doc at the Centre d'Optique, Photonique et Laser (COPL), Université Laval, Québec, Canada. His projects focus on optical coherent detection systems with higher-order modulation formats, OFDM-over-fiber and full-duplex wireless-fiber interfacing. He is currently with Infinera Corp., California, United States, as a test developing engineer for new generations of photonic integrated circuit employed in coherent long-haul and metro communication systems.

Leslie Ann Rusch (S'91-M'94-SM'00-F'10) received the B.S.E.E. degree (with honors) from the California Institute of Technology, Pasadena, in 1980 and the M.A. and Ph.D. degrees in electrical engineering from Princeton University, Princeton, NJ, in 1992 and 1994, respectively.

Dr. Rusch has experience in defense, industrial and academic communications research. She was a communications project engineer for the Department of Defense from 1980-1990. While on leave from Université Laval, she spent two years (2001-2002) at Intel Corporation creating and managing a group researching new wireless technologies. She is currently a Professor in the Department of Electrical and Computer Engineering at Université Laval, QC, Canada, performing research on wireless and optical communications. She is a member of the Centre for Optics, Photonics, and Lasers (COPL) at Université Laval. Prof. Rusch's research interests include digital signal processing for coherent detection in optical communications, spatial multiplexing using orbital angular momentum modes in fiber, radio over fiber and OFDM for passive optical networks; and in wireless communications, optimization of the optical/wireless interface in emerging cloud based computing networks, optical pulse shaping for high-bit rate ultrawide-band (UWB) systems, and implantable medical sensors with high bit rate UWB telemetry.

Dr. Rusch is recipient of the IEEE Canada J. M. Ham Award for Graduate Supervision. Prof. Rusch has published over 100 journal articles in international journals (90\% IEEE/IEE) with wide readership, and contributed to over 140 conferences. Her articles have been cited over 3800 times per Google Scholar.

Sophie LaRochelle (M'00) received a Bachelor's degree in engineering physics from Université Laval, Canada, in 1987; and a Ph.D. degree in optics from the University of Arizona, USA, in 1992.

From 1992 to 1996, she was a Research Scientist at the Defense Research and Development Canada - Valcartier, where she worked on electro-optical systems. She is now a professor at the Department of Electrical and Computer Engineering, Université Laval, where she holds a Canada Research Chair (Tier 1) in Advanced Photonics Technologies for Communications. Her current research activities are focused on active and passive components for optical communication systems including silicon photonic devices, Bragg gratings filters, multi-wavelength and pulsed fiber lasers. Other research interests include optical fibers and amplifiers for spatial division multiplexing, all-optical signal processing and routing, and transmission of radio-over-fiber signals including UWB and GPS.

Dr. LaRochelle is an IEEE senior member and an OSA Fellow.